AAC Journals.ASM.org

Variations of Subunit ε of the *Mycobacterium tuberculosis* F_1F_o ATP Synthase and a Novel Model for Mechanism of Action of the Tuberculosis Drug TMC207

Goran Biuković,[a] Sandip Basak,[a] Malathy Sony Subramanian Manimekalai,[a] Sankaranarayanan Rishikesan,[a] Manfred Roessle,[b] Thomas Dick,[c] Srinivasa P. S. Rao,[d] Cornelia Hunke,[a] Gerhard Grüber[a]

School of Biological Sciences, Nanyang Technological University, Singapore, Republic of Singapore[a]; European Molecular Biology Laboratory, Hamburg Outstation, EMBL c/o DESY, Hamburg, Germany[b]; National University of Singapore, Yong Loo Lin School of Medicine, Department of Microbiology, Singapore, Republic of Singapore[c]; Novartis Institute for Tropical Diseases Pte. Ltd., Singapore, Republic of Singapore[d]

The subunit ε of bacterial F_1F_O ATP synthases plays an important regulatory role in coupling and catalysis via conformational transitions of its C-terminal domain. Here we present the first low-resolution solution structure of ε of *Mycobacterium tuberculosis* (*Mt*ε) F_1F_O ATP synthase and the nuclear magnetic resonance (NMR) structure of its C-terminal segment ($Mt\varepsilon_{103–120}$). *Mt*ε is significantly shorter (61.6 Å) than forms of the subunit in other bacteria, reflecting a shorter C-terminal sequence, proposed to be important in coupling processes via the catalytic β subunit. The C-terminal segment displays an α-helical structure and a highly positive surface charge due to the presence of arginine residues. Using NMR spectroscopy, fluorescence spectroscopy, and mutagenesis, we demonstrate that the new tuberculosis (TB) drug candidate TMC207, proposed to bind to the proton translocating *c*-ring, also binds to *Mt*ε. A model for the interaction of TMC207 with both ε and the *c*-ring is presented, suggesting that TMC207 forms a wedge between the two rotating subunits by interacting with the residues W15 and F50 of ε and the *c*-ring, respectively. T19 and R37 of ε provide the necessary polar interactions with the drug molecule. This new model of the mechanism of TMC207 provides the basis for the design of new drugs targeting the F_1F_O ATP synthase in *M. tuberculosis*.

With one-third of humankind infected subclinically, an incidence of nine million new cases of active tuberculosis disease (TB), and two million deaths per year, *Mycobacterium tuberculosis* remains the most important bacterial pathogen in the world (1). The increased prevalence of coinfections with HIV and the infection with multidrug-resistant as well as extensively drug-resistant mycobacterial strains are contributing to the worsening impact of this disease (2). New drugs for TB, which should have a new mechanism of action to be active against drug-resistant TB, are urgently needed. Furthermore, they should be active against the dormant form of the pathogen to enable shortening of the lengthy regimens currently in use (3). TMC207, the first member of a promising new class of antimycobacterial drugs, the diarylquinolines, is in early clinical development (4). The compound is active against drug-resistant *M. tuberculosis* and—importantly—also bactericidal for the phenotypically drug-resistant dormant form of the bacillus (5). TMC207 was identified in a phenotypic whole-cell screen. Target deconvolution studies revealed that the candidate interferes with the enzyme machinery responsible for the synthesis of the biological fuel ATP (5–7). Chemical inhibition of ATP synthesis by diarylquinoline strongly decreased the cellular ATP level, leading to death in not only replicating but also nonreplicating persistent mycobacteria (5, 6). The diarylquinoline TMC207 represents the first pharmacological proof that mycobacterial ATP synthesis can be a target of intervention (8). Furthermore, it demonstrates that ATP synthase is essential for the viability of growing as well as nongrowing dormant mycobacteria. These findings were additionally supported by physiological studies of a deletion mutant of *atpD*, encoding the β subunit of F_1F_o ATP synthase in *M. smegmatis* (9). Critically, the excellent efficacy of TMC207 in a proof-of-concept study validates this target clinically. Of note, the drug displays pronounced target selectivity, with an extremely low effect on ATP synthesis in the human enzyme (10).

The target of TMC207, the mycobacterial F_1F_O ATP synthase (5), consists of the ATP-synthesizing F_1 and the proton-translocating F_O part (subunits $a_1b_2c_{9-15}$ [11]). The proton transfer in the F_O sector is linked via the central stalk subunits γ and ε to the $\alpha_3\beta_3$-catalytic hexamer of F_1 (11, 12). This coupling event is achieved by binding of the N-terminal domain of ε to the rotating subunit γ and the *c*-ring (Fig. 1A), as well as the interactions of the C termini of both ε and γ with the nucleotide-binding subunits α and β, which form the catalytic interfaces (12, 13).

In bacteria and plants, subunit ε consists of an N-terminal β-barrel and a C-terminal segment, composed of two α-helices (14–16). As shown in the isolated (15) as well as in the F_1-bound (17) complex, these two C-terminal α-helices can either be folded in a hairpin form and sitting on top of the N-terminal domain (NTD) (Fig. 1A and B), called the compact state (ε_c), or extended (ε_e [17]). In such an extended state, ε interacts with the same five subunits, α1, α2, β1, β3, and γ, as the inhibitor protein of the mitochondrial F_1F_O ATP synthase (18), causing enzymatic inhibition. The ε_c and ε_e states are described to be dependent on nu-

Received 13 May 2012 Returned for modification 27 July 2012
Accepted 11 October 2012
Published ahead of print 22 October 2012
Address correspondence to Gerhard Grüber, ggrueber@ntu.edu.sg.
Supplemental material for this article may be found at http://dx.doi.org/10.1128/AAC.01039-12.

doi:10.1128/AAC.01039-12

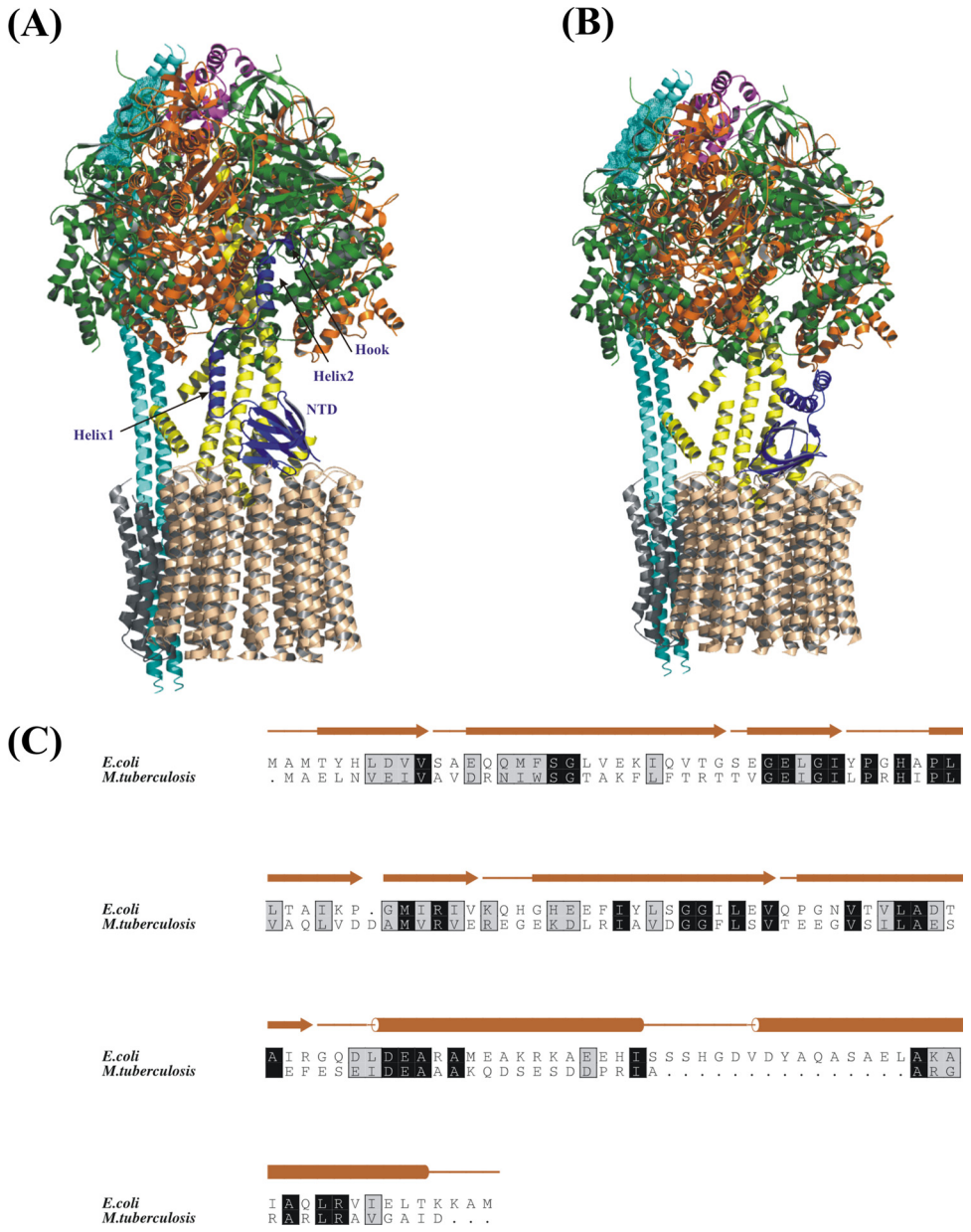

FIG 1 Proposed model of the *E. coli* F_1F_O ATP synthase enzyme complex. The structures of α (green), β (orange), and γ (yellow) subunits (Protein Data Bank [PDB] ID: 1D8S), the ε subunit (blue) (PDB ID: 1BSN), the N-terminal domain (NTD) of the δ_{1-134} subunit (magenta) (PDB ID: 1ABV), the model of the *c*-ring (brown) with subunit *a* (gray) (PDB ID: 1C17), and the subunit *b* dimer model (cyan) were fitted. The subunit *b* model was created by fitting the NMR solution structures of b_{1-34} (45), b_{30-82} (PDB ID: 2KHK), and $b_{140-156}$ (46) and the crystallographic structure of b_{62-122} (PDB ID: 1L2P). The mesh in subunit *b* indicates the region for which the structure is not known. Model with *EC*ε in the extended (A) (17) and compact (B) conformations are shown. The N-terminal domain (NTD), helix 1, helix 2, and hook regions are indicated for *EC*ε. (C) Amino acid sequence alignment of *EC*ε and *Mt*ε. The secondary structure of *EC*ε is based on the NMR solution structure determined by Wilkens and Capaldi (15).

cleotide binding to the C-terminal helices of ε (16, 19) and the membrane potential (20). For some bacteria the ε_c state can be stabilized by binding of ATP, thus favoring active complexes when cellular ATP is abundant (21).

Functional ATP synthase is critical for the viability of pathogenic bacteria such as *M. tuberculosis*. Based on the physiological role of ε regulation in the ATP synthase, which is connected to the C-terminal segment of this subunit, bacteria show variations in length and composition of the amino acid sequence of this C terminus. This is also revealed by the shorter C-terminal region of the *M. tuberculosis* ε compared to the *Escherichia coli* form (Fig. 1C), described to be responsible for enzymatic activity (17), coupling (12), and modulation of nucleotide specificity in the catalytic sites (21).

So far no structural details are available for mycobacterial F_1F_O ATP synthase, its subunits, or the interaction site of the TB drug TMC207 inside the enzyme. In this study, we have employed a complementary approach of solution X-ray scattering and nuclear

magnetic resonance (NMR) spectroscopy to determine the solution structures of *M. tuberculosis* subunit ε and its C-terminal domain, respectively. Importantly, we describe for the first time that TMC207 does interact with the N-terminal domain of ε. We propose a new model, in which TMC207 binds like a wedge in the interface of ε and subunit *c* and blocks the rotary mechanism of the *c*-ring with the central stalk subunits of F_1.

MATERIALS AND METHODS

Production and purification of *Mt*ε and its mutant proteins *Mt*ε-T19A and *Mt*ε-R37G. The gene *atpC*, which codes for subunit ε of the F_1F_O ATP synthase from the strain *M. tuberculosis* H37Rv, was amplified by PCR in two steps. Restriction sites NcoI and SacI, which were used for cloning, were introduced by the following PCR primers: Forward *atpC*, 5′-GAGT TGTCCCATGGCCGAATTGAAC-3′; Reverse *atpC*, 5′-TCATCGAGCT CTTAGTCAATCGCGC-3′. In order to abolish restriction site NcoI, which is present in an *atpC* DNA sequence, the following pair of internal primers introducing a silent mutation was constructed: IF-NcoI, 5′-GAT GACGCAATGGTGCGGGTC-3′; IR-NcoI, 5′-GACCCGCACCATTGC GTCATC-3′. In the first step, PCR products were obtained in two independent reaction mixtures containing the primer pairs Forward *atpC*–IR-NcoI and IF-NcoI–Reverse *atpC*. The genomic DNA from the strain *M. tuberculosis* HR37v was used as the template. In the second PCR step, these products were used together as a template in a final reaction using primer pair Forward *atpC*–Reverse *atpC*. The mutated *atpC* genes coding for *Mt*ε-R37G and -T19A were obtained by PCR *in vitro* mutagenesis using cloned gene *atpC* as a template and the internal primer pairs IF-R37G (5′-CATCCTGCCAGGACACATTCCGT-3′)–IR-R37G (5′-ACGGAAT GTGTCCTGGCAGGATG-3′) and IF-T19A (5′-CATCTGGTCGGGTG CAGCGAAGT-3′)–IR-T19A (5′-ACTTCGCTGCACCCGACCAGATG-3′), respectively.

The purified PCR products were digested with restriction enzymes NcoI and SacI and ligated into the vector $pET9d_1$ (22). The DNA constructs were transformed into *Escherichia coli* cells [strain BL21(DE3)] and grown on kanamycin-containing Luria-Bertani (LB) agar plates. To express the cloned genes, liquid culture was shaken in LB medium containing kanamycin (30 μg ml^{-1}) for about 4 h at 37°C until an optical density at 600 nm (OD_{600}) of 0.6 to 0.7 was reached, and then expression was induced with isopropyl-β-D-thiogalactoside (IPTG) to a final concentration of 1 mM. The cells were lysed on ice by sonication in buffer A (50 mM Tris-HCl, pH 8.5, 200 mM NaCl, 10% glycerol, 4 mM Pefabloc SC [BIOMOL]). The precipitated material was separated by centrifugation at 10,000 × *g* for 35 min. The supernatant was passed over a Ni-nitrilotriacetic acid (Ni-NTA) resin column to isolate *Mt*ε. The His-tagged protein was allowed to bind to the matrix for 1.5 h at 4°C and eluted with an imidazole gradient (50 to 400 mM) in buffer A. Fractions containing *Mt*ε or the mutant ε-R37G were identified by SDS-PAGE, collected, and diluted to a final concentration of 100 mM NaCl. Filtered samples (0.45-μm pore size; Millipore) containing ε or its mutant protein were applied to anion-exchange Resource Q chromatography, which was previously equilibrated with 50 mM Tris-HCl, 100 mM NaCl, pH 8.5. Whereas monomeric *Mt*ε does not bind to the column matrix, the oligomeric forms of ε together with impurities bind to the column. Eluted *Mt*ε was concentrated by using Centricon YM-3 (3-kDa molecular mass cutoff) spin concentrators (Millipore), and aliquots of 1 ml were subjected to gel filtration chromatography using a Superdex 75 HR 10/30 column (Amersham Biosciences), which was previously equilibrated with a buffer of 50 mM Tris-HCl (pH 8.5), 200 mM NaCl, 10% glycerol. The fractions containing subunit ε and the mutant proteins ε-T19A and ε-R37G were collected and concentrated to the required concentrations.

Peptide synthesis of $\varepsilon_{103–120}$. The peptide $\varepsilon_{103–120}$ from *M. tuberculosis* (strain $H37R_V$), composed of the amino acid sequence $_{103}$DPRIAAR GRARLRAVGAI$_{120}$, was synthesized and purified by reversed-phase high-pressure liquid chromatography at the Division of Chemical Biology and Biotechnology, School of Biological Sciences, Nanyang Technological University, Singapore. The purity of the peptide was confirmed by electrospray ionization (ESI) mass spectrometry.

CD spectroscopy of *Mt*ε and mutant proteins *Mt*ε-T19A and *Mt*ε-R37G as well as $Mt\varepsilon_{103–120}$. Steady-state CD spectra were measured in far-UV light (185 to 260 nm) using a Chirascan spectropolarimeter (Applied Photophysics) as described previously (23). Circular dichroism (CD) spectroscopy of *Mt*ε, *Mt*ε-T19A, and *Mt*ε-R37G (1.0 mg/ml) and the peptide $\varepsilon_{103–120}$ (2.0 mg/ml) was performed in buffer A (50 mM Tris-HCl, pH 8.5, 200 mM NaCl, 10% glycerol) and buffer B (25 mM phosphate, pH 6.5, 50% TFE [4-chlorobutanol and 2,2,2-trifluoroethanol]), respectively. The spectrum for the buffer was subtracted from the spectrum of the protein, and the data were analyzed as described recently (24).

X-ray scattering experiments and data analysis of subunit ε. Small-angle X-ray scattering data for *Mt*ε were collected on the X33 SAXS camera of the EMBL Hamburg located on a bending magnet (sector D) on the storage ring DORIS III of the Deutsches Elektronen Synchrotron (25) The scattering patterns from *Mt*ε were measured at protein concentrations of 3.0 and 6.0 mg/ml. Protein samples were prepared in 50 mM Tris-HCl (pH 8.5), 200 mM NaCl, 10% glycerol as a radical quencher. The data were normalized to the intensity of the incident beam; the scattering of the buffer was subtracted, and the difference curves were scaled for concentration. All the data processing steps were performed using the program package PRIMUS (26). The forward scattering, $I(0)$, and the radius of gyration, R_g, were evaluated using the Guinier approximation (27). The molecular mass of *Mt*ε was calculated by comparison with the forward scattering from the reference solution of bovine serum albumin (BSA). From this procedure a relative calibration factor for the molecular mass can be calculated using the known molecular mass of BSA (66 kDa) and the concentration of the reference solution. The shape of subunit ε in solution was built by the program GASBOR (28, 29). *Ab initio* shape models for subunit ε were obtained by superposition of 10 independent GASBOR reconstructions.

NMR spectroscopy of $Mt\varepsilon_{103–120}$. Peptide $\varepsilon_{103–120}$ (2 mM) was dissolved in 25 mM phosphate buffer at pH 6.5 and 50% d_2TFE (deuterated 2,2,2-trifluoroethanol). All spectra were obtained at 298 K on a 600-MHz Avance Bruker NMR spectrometer, equipped with actively shielded cryoprobe and pulse field gradients. Total correlation spectroscopy (TOCSY) and nuclear Overhauser effect spectroscopy (NOESY) spectra of the peptide were recorded with mixing times of 80 and 250 ms, respectively. DSS (2,2-dimethyl-2-silapentane-5-sulfonate sodium salt) was used as an internal reference. All the data acquisition and processing were done by the TopSpin (Bruker Biospin) program. The Sparky suite was used for spectrum visualization and peak picking. Standard procedures based on spin-system identification and sequential assignment were adopted to identify the resonances. Interproton distances were obtained from the NOESY spectra by using the caliba script included in the CYANA 2.1 package (30). Dihedral angle restraints were derived from TALOS. The predicted dihedral angle constraints were used for structure calculation, with a variation of ±30° from the average values. The CYANA 2.1 package was used to generate the three-dimensional (3D) structure of the peptide. Several rounds of structural calculation were performed. Angle and distance constraints were adjusted until no NOE violations occurred. In total, 100 structures were calculated and an ensemble of 20 structures with lowest total energy was chosen for structural analysis.

Titration of *Mt*ε against drugs through NMR spectroscopy. To analyze possible interactions of *Mt*ε with drugs (TMC207 or mefloquine/HCl), a series of ^1H-^{15}N HSQC (hetero-nuclear single quantum coherence) spectra were recorded at 303 K for a fixed concentration of *Mt*ε (250 μM) and with increasing concentrations of the drugs, respectively (up to 2.0 equivalents). *Mt*ε was prepared in 50 mM sodium phosphate (pH 6.5) buffer containing 200 mM NaCl and 10% glycerol. The protein was incubated for 30 min with the drug at each level of concentration. Any changes in the chemical shift were monitored on the HSQC spectra.

Tryptophan fluorescence spectroscopy of *Mt*ε, *Mt*ε-T19A, and *Mt*ε-R37G in the presence of the antibiotic TMC207. A Varian Cary Eclipse spectrofluorometer was used, and all experiments were carried out at 20°C. The samples were excited at 295 nm, and the emission spectrum was recorded from 310 to 430 nm with excitation and emission bandpasses set to 5 nm and a scan rate of 30 nm/min. For titration of the tryptophan fluorescence of *Mt*ε as well as the mutant proteins *Mt*ε-T19A and *Mt*ε-R37G with compound TMC207, the peak emission wavelength was 339 nm. Before use, subunit ε or the mutant forms *Mt*ε-T19A and *Mt*ε-R37G and defined concentrations of compound TMC207 were incubated in a buffer of 50 mM Tris-HCl (pH 8.5), 200 mM NaCl, 18% dimethyl sulfoxide (DMSO), and 10% glycerol for 20 min. After measurements, the raw fluorescence spectra were corrected for the buffer values.

Isothermal titration calorimetry of *Mt*ε and nucleotides. The binding affinities of *Mt*ε toward nucleotides ATP or ADP was examined by isothermal titration calorimetry (ITC) in a MicroCal iTC200 microcalorimeter (MicroCal, Northampton, United Kingdom). Both the protein and the nucleotides were equilibrated in the same buffer (50 mM Tris-HCl, 200 mM NaCl, 10% glycerol, pH 8.5), filtered, and degassed before titration. The solution, containing either 1 mM ATP or 1 mM ADP and 1 mM Mg^{2+}, was titrated in 1-μl injections against 10 μM protein solution, which was loaded in the sample cell. The experiment was performed as described recently (31). The control experiment was done under the same experimental conditions using 10 μM protein of subunit A from the archaeon *Pyrococcus horikoshii* OT3 in buffer, composed of 50 mM Tris-HCl, pH 7.5. Data analysis was done as described recently (31).

Protein structure accession number. The Protein Data Bank accession code of the peptide $Mt\varepsilon_{103–120}$ is 2LX5.

RESULTS

Purification of recombinant subunit ε and its secondary structural content. Recombinant subunit ε of the *M. tuberculosis* H37Rv F_1F_O ATP synthase was isolated to high quality and quantity using Ni-NTA-affinity, ion, and size exclusion chromatography (see Fig. S1A in the supplemental material). The molecular mass of the recombinant protein was analyzed by matrix-assisted laser desorption ionization (MALDI) mass spectrometry, revealing that the protein has a sequence-based predicted mass of 15.19 kDa. The proper secondary folding of the recombinant *Mt*ε was studied by circular dichroism (CD) spectroscopy, resulting in a secondary structural content of 21% α-helix and 58% β-sheet (see Fig. S1B in the supplemental material). In order to prove whether the recombinant protein is able to bind to the $\alpha_3\beta_3\gamma$ complex, fluorescence correlation spectroscopy (FCS) experiments were performed and are described in the supplemental material. The autocorrelation curves of the fluorescently labeled *Mt*ε with increased concentrations of $\alpha_3\beta_3\gamma$ of the related thermophilic F_1F_O ATP synthase from *Bacillus PS3* (see Fig. S2A in the supplemental material) and the resulting concentration-dependent binding curve are shown in the supplemental material (see Fig. S2B). The increase of the mean diffusion time, τ_D, reflects the increase in the mass of the diffusing particle, due to the formation of the Atto488-ε-$\alpha_3\beta_3\gamma$ complex. A binding constant of 4.0 μM was determined by nonlinear curve fit by the Hill equation.

Low-resolution structure of *Mt*ε in solution. The high purity and mono-dispersity of the protein are nicely indicated by small-angle X-ray scattering (SAXS) data, represented by the final composite scattering curve in Fig. 2A. The radius of gyration, R_g, and the maximum dimension, D_{max}, of subunit ε were 17.6 ± 0.3 Å and 61.7 ± 1 Å, respectively (Fig. 2B). Comparison with the scattering from the reference solutions of BSA yields an estimated molecular mass of 15.7 kDa. The gross structure of *Mt*ε was restored *ab initio* from the scattering pattern in Fig. 2A using the dummy residues modeling program GASBOR (26), which fitted well to the experimental data in the entire scattering range (a typical fit displayed in Fig. 2A, red curve, has the discrepancy χ^2 = 1.17). Ten independent reconstructions yielded reproducible models, and the best model is displayed in Fig. 2C. Qualitative analysis of the distance distribution function suggests that subunit ε consists of a major portion, yielding a principal maximum in the $p(r)$ around 20 Å (Fig. 2B), whereas the separated protuberance domain gives rise to a shoulder from 42 Å to 61.7 Å. The protein appears as a two-domain molecule with a large major domain of about 39 by 27 Å, whereby the elongated domain has a dimension of about 20 by 11 Å. The gross structure of the globular domain resembles very much the shape of the N-terminal domain of the solution NMR structure of the homolog ε subunit of the *E. coli* F_1F_O ATP synthase, and this N-terminal barrel of *EC*ε is well accommodated within the globular domain of *Mt*ε (Fig. 2D). In contrast, the elongated domain (20 Å) of *Mt*ε is shorter than that of the *EC*ε subunit (30 Å [32]), reflecting the loss of 15 amino acids in the C terminus of *Mt*ε (Fig. 1C).

Solution structure of the C-terminal segment $\varepsilon_{103–120}$. To get a deeper insight into the very C-terminal region of *M. tuberculosis* subunit ε, the C-terminal segment $_{103}$DPRIAARGRARLRAVGAI$_{120}$ was synthesized and the CD spectrum shows an α-helical content of 87% (see Fig. S3A in the supplemental material). In order to determine the 3D structure of $Mt\varepsilon_{103–120}$, the primary sequences of $\varepsilon_{103–120}$ were sequentially assigned as per the standard procedure by using a combination of TOCSY and NOESY spectra (see Fig. S3B and C in the supplemental material). Secondary structure prediction was done by using the PREDITOR online program (33), which uses HA chemical shifts and reveals the presence of an α-helical structure (see Fig. S4A in the supplemental material). Out of 100 structures generated, the 20 lowest-energy structures were taken for further analysis. In total, an ensemble of 20 calculated structures resulted in an overall mean root square deviation (RMSD) of 0.20 Å for the backbone atoms and 1.09 Å for the heavy atoms (Fig. 3A). All these structures have energies lower than −100 kcal mol^{-1}, with no NOE violations and no dihedral violations. The summary of the statistics for 20 structures are shown in Table S1 in the supplemental material. Identified cross peaks in the HN-HN and HA-NH regions are shown in Fig. S4B in the supplemental material. From the assigned NOESY spectrum HN-HN, Hα-HN (i, i + 3), Hα-HN (i, i + 4), and Hα-Hβ (i, i + 3) connectivities were plotted and support α-helical formation in the structure. The calculated structure has a total length of 27.46 Å and displays an α-helical region between residues 104 and 119 (23.31 Å; Fig. 3B). Molecular surface electrostatic potential of the peptide is shown in Fig. 3C, where positive charge residues R109 and R113 were distributed on one side and R111 as well as R115 on the opposite side of the helix. The solution structure of $\varepsilon_{103–120}$ was positioned inside the elongated domain of the solution shape of *Mt*ε. As revealed in Fig. 2D, $Mt\varepsilon_{103–120}$ fits well into the extended domain, with an RMSD of 0.29 Å.

Probing the interaction of nucleotides with *Mt*ε. In bacteria and in chloroplasts the C terminus of ε is described as a mobile regulatory element that alters its conformation in response to nucleotide conditions or the ion motive force (IMF) (2, 20). ATP binding in ε of thermophilic *Bacillus* PS3 and *Bacillus subtilis* forces the C-terminal helices into a hairpin conformation, which extends in the absence of the nucleotide, leading to an inhibited

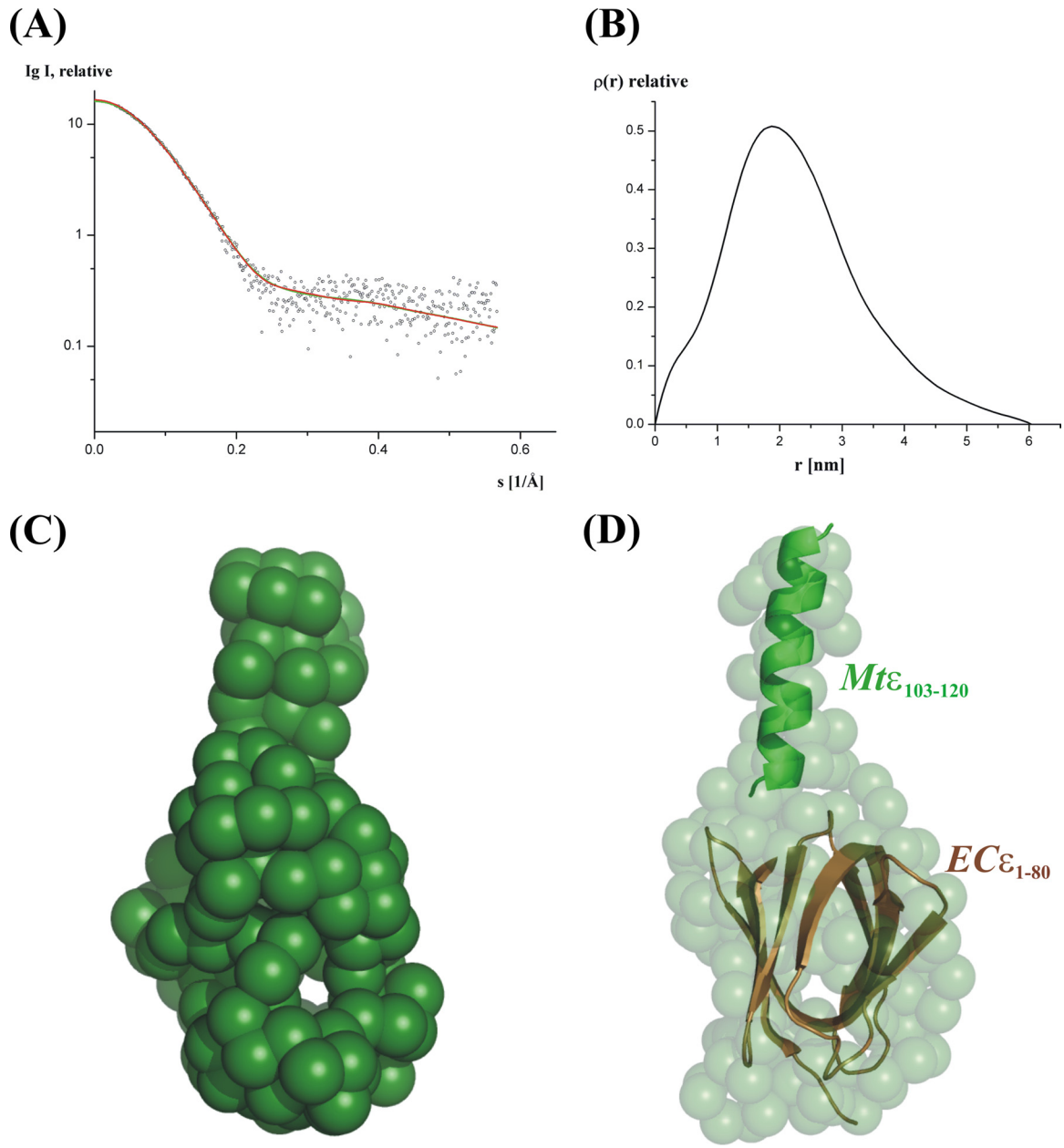

FIG 2 Small-angle X-ray scattering data of *Mt*ε. (A and B) Experimental scattering curves (A) and distance distribution functions (B) of *Mt*ε. (C) Low-resolution structures of *Mt*ε. (D) Superimposition of the low-resolution solution structure of *Mt*ε with the N-terminal β-barrel structure of *EC*ε (37) (brown) and the $Mt\varepsilon_{103–120}$ (green) peptide structure.

ATP hydrolysis state (19). Here we performed isothermal titration calorimetry (ITC) to investigate whether the *M. tuberculosis* subunit ε also binds nucleotides. As demonstrated in the injection profile of *Mt*ε (see Fig. S5A and C in the supplemental material) after baseline correction (top panel) with the profile of heat release/mole of injected ligand (bottom panel), the subunit binds neither ATP nor ADP. As shown by a control experiment under the same conditions, subunit A of the *Pyrococcus horikoshii* OT3 A_1A_O ATP synthase binds MgATP and MgADP with K_d values of 3 μM and 2.1 μM, respectively (see Fig. S5B and D in the supplemental material), which is in good agreement with previous results (31).

The drug TMC207 interacts with *Mt*ε. In all types of F_1F_O ATP synthases the N-terminal domain of ε binds to the rotating subunit γ and directly couples to the *c*-ring of the membrane-embedded F_O-sector (12). The TB drug candidate TMC207 has been proposed to bind to subunit *c* by acting independently of the proton motive force and would not compete with protons for a common binding site, indicating that TMC207 may interfere with conformational changes in the entire enzyme, like the rotation of the *c*-ring (34). Based on these suggestions and the direct coupling of both the *c*-ring and subunit ε in the rotary events, we asked whether TMC207 may interact also with *M. tuberculosis* subunit ε. In order to demonstrate ε-TMC207 binding, NMR titration ex-

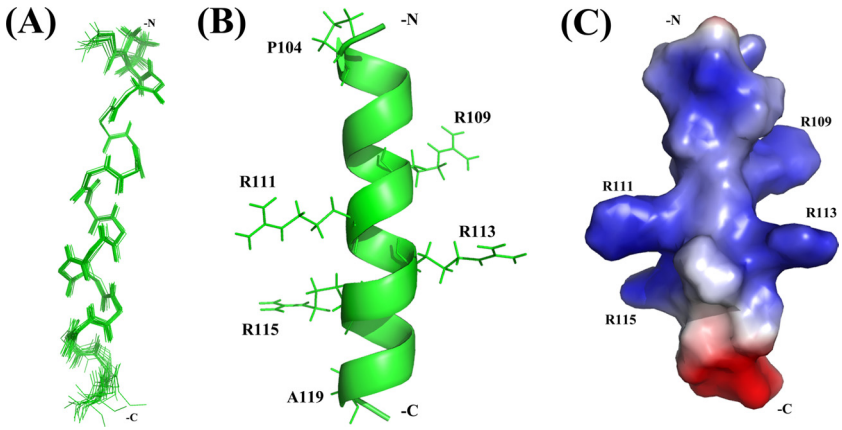

FIG 3 NMR studies of the peptide $Mt\varepsilon_{103–120}$.(A) Superimposition of the 20 lowest-energy NMR structures of $Mt\varepsilon_{103–120}$ in line representation. (B) Average NMR structures of $Mt\varepsilon_{103–120}$ in cartoon representation. (C) Molecular surface electrostatic potential of peptide $Mt\varepsilon_{103–120}$ generated by Pymol, where the positive potentials are drawn in blue and the negative in red.

periments were performed. ^{15}N-labeled protein was used to acquire the HSQC spectrum of *Mt*ε. The HSQC spectrum showed a good dispersion of around 4 ppm at 303 K, with acquisition giving a total of 126 peaks (Fig. 4A). When the ^{15}N-labeled *Mt*ε was titrated against increasing concentration of TMC207, seven peaks showed distortion at a molar ratio of 1:1. These peaks, namely 5, 9, 15, 16, 18, 24, and 105 (Fig. 4A), showed further dislocation on the spectrum upon titration against a 1:2 molar ratio and some peaks disappeared, giving an indication of the drug binding to ε. The predominant peaks, showing more distortions, are shown on the top left corner of the spectrum as an insert in Fig. 4A. Peak number 105, which appears at 10 ppm, can be identified as the tryptophan residue W15, based on the chemical shift index (35). Changes in this resonance of the W15 peak upon the addition of TMC207 indicate its significant interaction. On the other hand, no peak distortion was observed when *Mt*ε was titrated against the mefloquine hydrochloride at a molar ratio of 1:2 (see Fig. S6 in the supplemental material), reflecting the specific interaction of TMC207 with *M. tuberculosis* ε. Mefloquine was used in the experiment, as it has been shown to target the F_O complex of the F_1F_O ATP synthase of *Streptococcus pneumoniae* (36).

Since the NMR titration experiment of *Mt*ε with TMC207 has shown that the only tryptophan residue (W15) of ε undergoes a shift in the HSQC spectra after addition of the compound, we used intrinsic tryptophan fluorescence spectroscopy to confirm and to quantitatively evaluate the binding of TMC207 to *Mt*ε. The corrected tryptophan fluorescence spectrum of *Mt*ε reveals the emission maximum at 339 nm (Fig. 4B). The intensity dropped by 34% and the maximum of the peak shifted to a longer wavelength, indicating an alteration in the close proximity of W15 after addition of TMC207. To quantitate the spectra, the binding of TMC207 to ε was measured using fluorescence quenching at 339 nm. As shown in the titration curve of Fig. 4C, a binding constant of 19.1 μM could be determined.

A plausible model for the interaction of the TMC207 molecule with both ε and the *c*-ring was generated (Fig. 4D). The crucial residues, which are on the interface between ε and the *c*-ring, were identified in the *E. coli* structure and were changed to their respective residues in the *M. tuberculosis* sequence, after which the TMC207 molecule was modeled in the interface of ε and the *c*-ring (Fig. 4D, right). The model shows that the TMC207 molecule forms a wedge between the two subunits by interacting with the residues W15 and F50 of ε and the *c*-ring, respectively. Two other residues, T19 and R37 of ε, which are within 5 Å of the TMC207 molecule and are shown in the presented data to be important in TMC207-ε binding (see below), might give the necessary polar interaction to the drug molecule.

To confirm the binding model, residues T19 and R37 of *Mt*ε were replaced by alanine and glycine residues, respectively, which were allocated in the corresponding positions of *EC*ε (Fig. 1C). Tryptophan titrations of the R37G mutant proteins revealed that a significant drop and shift of the tryptophan spectrum could be achieved only at a concentration of 48 μM TMC207, which was identical for the *Mt*ε-T19A mutant form (not shown). These data indicate that binding of TMC207 to *Mt*εT19A or *Mt*εR37G is strongly affected by these mutations and support the importance of the residues T19 and R37 in TMC207 binding (see Fig. S1D in the supplemental material).

DISCUSSION

The presented NMR structure of the *M. tuberculosis* C-terminal $\varepsilon_{103–120}$ shows an α-helical stretch between the residues P104 and A119. When superimposed into the low-resolution structure of the *Mt*ε this α-helical structure fits well in the extended domain of *Mt*ε (RMSD of 0.297Å [Fig. 2D]). Compared to the ε-inhibited state, ε_e, in the *EC*F_1 ATPase (Fig. 5), which blocks both hydrolysis and synthesis of ATP (17), *Mt*ε, with its shorter C-terminal domain, will not reach the upper region of the α-β interface close to the adenine-binding pocket and the N-terminal and rotating part of γ (17). The surface potential of $Mt\varepsilon_{103–120}$ reveals a highly positive surface charge due to the presence of arginine residues, with R109 and R113 situated on one side and R111 and R115 located on the opposite side (Fig. 3C). The two unique residues R111 and R113 on both sides of the *Mt*ε C-terminal helix give the helix a very positive surface, enabling this region to interact strongly with the C terminus of one of the catalytic subunits and thereby regulate catalytic processes. As demonstrated recently, the very C terminus of *Mt*ε in ATP synthases of slow- and fast-growing mycobacteria is responsible for blocking of ATP hydrolysis, preventing excess ATP consumption under low oxygen tensions (37). These studies also

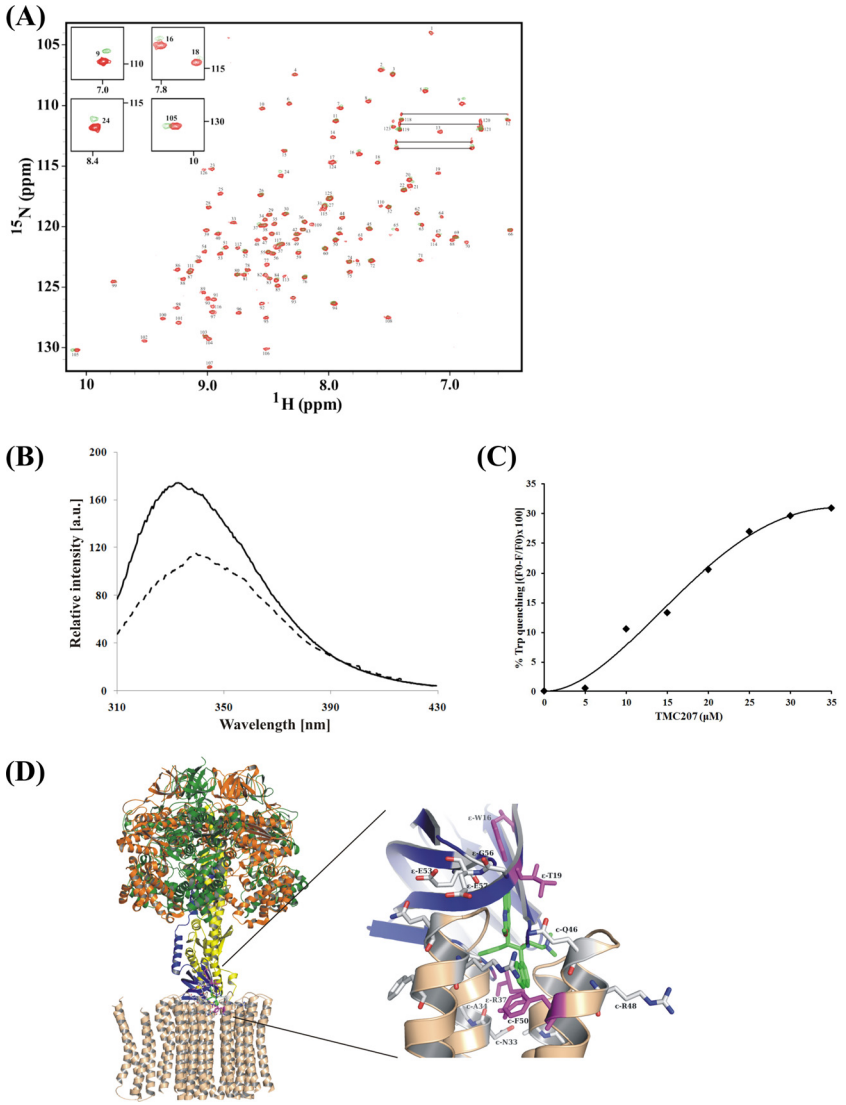

FIG 4 Spectroscopic titration studies of *Mt*ε with TMC207. (A) 2D ^{1}H-^{15}N-HSQC spectra of *Mt*ε in the absence (red) and presence (green) of 2 equivalents of drug (TMC207). The HSQC spectra were acquired at 303 K with 250 μM protein dissolved in 50 mM sodium phosphate (pH 6.5) buffer containing 200 mM NaCl and 10% glycerol. The peaks showing chemical shift change upon addition of the drug are shown in the respective insets. (B) Intrinsic tryptophan fluorescence titration of *Mt*ε in the absence (solid line) and presence (broken line) of TMC207. Excitation was at 295 nm. (C) Fluorescence titration of *Mt*ε with TMC207. Excitation was at 295 nm, and the emission was measured at 339 nm. (D) Model of the *EC*F$_1$ ATPase structure (17) with the *c*-ring (PDB ID: 1C17) and part of subunit *a* (PDB ID: 1C17) (left) and a plausible model showing the interaction of TMC207 (green) with the ε subunit (blue) and *c*-ring (beige) (right). The model shows the nonhomologous residues between *Mt*ε and *E. coli* ε and *c* subunits, changed to *M. tuberculosis* residues, shown in gray and magenta stick representation. The crucial residues that might interact with the TMC207 molecule are shown in magenta stick representation for *Mt*ε and the *c*-ring. The TMC207 molecule is proposed to interact with W15 of *Mt* ε and F50 of the *c*-ring.

demonstrated that suppression of hydrolytic activity appeared to be more pronounced in the slow-growing mycobacteria, reflecting an adaptation to environments with a low energy supply and/or decreased oxygen tension, such as that found in TB lesions in the lungs (38). Mycobacteria require oxygen for growth; however, they are capable of persisting in a quiescent form under anaerobic conditions. Similar ATP hydrolysis inhibition processes are reported for the obligate aerobic bacteria *Paracoccus denitrificans* (39) and *Micrococcus luteus* (40), whose ATP synthases show variations in the inhibitory subunits, which are represented by the *Pd*ξ (41) and the *Ml*δ subunit (42). Based on the specificity of the C-terminal segment of *Mt*ε and the variability of the C termini of bacterial ε as well as the diversity of inhibitory proteins in F_1F_O ATP synthases described above, the C-terminal domain of *Mt*ε becomes a promising epitope for compounds to bind and to regulate the synthesis of ATP but also to stimulate ATP hydrolysis.

In bacterial F_1F_O ATP synthases, the rotor of the F_1 motor and the rotor of the F_O motor are generally considered to be comprised, respectively, of the γ-ε subunit pair and the *c*-ring (35). The interface between subunits *c* and ε is formed by the loop region of the hairpin-structured *c* subunit and the bottom of the N-terminal β-barrel of ε (12). Proton transport via the subunit *a*-*c* interface triggers rotation of the oligomeric *c*-ring that is coupled to rotation of the γ-ε pair, which finally drives the synthesis in the

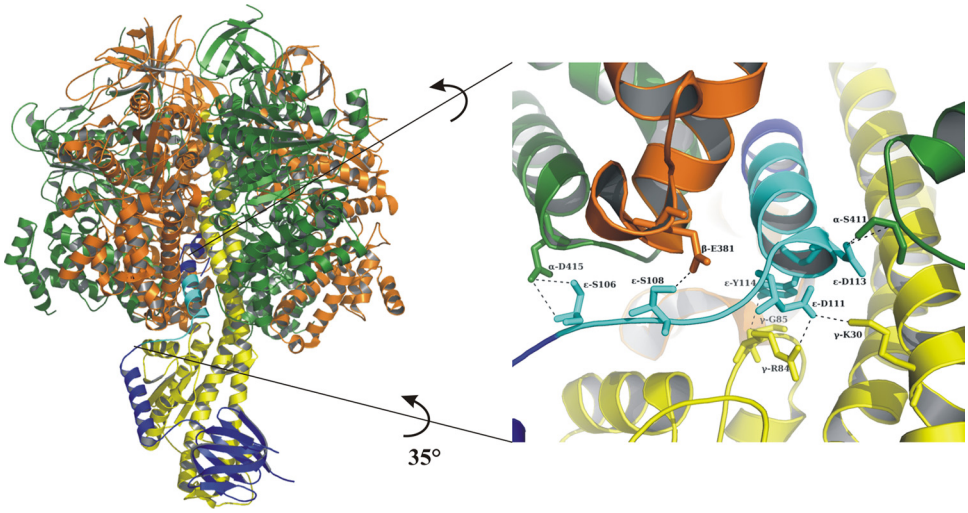

FIG 5 High-resolution model of ε with complex α3/β3 from *E. coli*. The recently determined crystal structure of the *E. coli* F_1 ATPase (17) revealed the coupling and inhibitory subunit ε in an extended state (left), in which the second loop and helix of the C-terminal segment of ε contact α1, α2, β1, β3, and γ, with helix 2 inserting into the central rotary cavity of the $\alpha_3\beta_3$-hexamer (right). The structure on the right is shown rotated by 35° for better viewing.

$\alpha_3\beta_3$-hexamer. Based on docking studies TMC207 has been predicted to bind at the *a*-*c* interface (5). Previously, the compound was proposed to block rotary movements of subunit *c* by interfering with conformational changes of subunit *c* during ATP catalysis, by competing with the protons for binding to *c*, or translocating across the membrane into the cytoplasm (43). Haagsma and colleagues have demonstrated that TMC207 does not directly compete with protons for a common binding site (34) and concluded that the protonated TMC207 may interfere with conformational changes in the F_1F_O ATP synthase. Based on docking studies the TMC207 molecule has been predicted to bind to the hydrophobic part of subunit *c* (5), which has been confirmed by recent binding studies using surface plasmon resonance spectroscopy using single subunit C from *M. tuberculosis* (5). The presented NMR titration experiments of *Mt*ε with TMC207 and mefloquine hydrochloride demonstrate that TMC207 does in addition specifically bind to the *Mt*ε subunit. The calculated binding constant K_d of 19.1 μM as well as the very weak TMC207 interaction of mutants *Mt*ε-T19A and *Mt*ε-R37G supports the specific interaction of the drug with the regulatory ε subunit. The data also identify W15 and R87 as interacting residues (Fig. 4C). Based on the results described above and the elongated character of TMC207 (13.3 Å by 8.55 Å), we propose that the drug TMC207 affects the catalysis of ATP formation by binding to both subunit *c* and ε, which together form a part of the rotary elements of the two motors F_O and F_1. As shown in Fig. 4D, TMC207 is predicted to work like a wedge which hinders the rotary movement of the *c*-ring as a consequence of proton translocation and conformational alteration in the membrane-integrated helices of *c*. As a further consequence, subunit ε is unable to regulate the efficiency of coupling, to influence the catalytic pathway, or to modulate nucleotide specificity in the catalytic sites (21). This new model would explain why TMC207 does not compete with protons for a common binding site (34).

In conclusion, the structural details of *Mt*ε add to nature's evolutionary strategy of varied key structural domains, along with the regulatory and inhibitory subunit ε of bacterial F_1F_O ATP synthases, or functionally homologue proteins, as described for IF1 (18), *Pd*ξ (44), and the *M. luteus* δ subunit (42). The alterations of the C-terminal segment of *Mt*ε may present a new target, to design new leads with improved antibacterial activities. In addition, the new insight into the interaction of TMC207 in the *c*-ε interface not only sheds light on the binding site of the drug but also adds to the mechanistic understanding of how the compound may act as an antibacterial in the *M. tuberculosis* F_1F_O ATP synthase. This forms a new platform to fine-tune the effect of TMC207 or to develop new compounds whose chemical as well as 3D traits will improve the effect of the wedge-shaped inhibitor and thereby the blocking of coupling events in the recently discovered TB drug target ATP synthase (5).

ACKNOWLEDGMENTS

Sandip Basak is grateful to the Nanyang Technological University for awarding a research scholarship. This research was supported by the New Initiative Fund FY2010, NTU.

REFERENCES

1. **Guillemont J, Meyer C, Poncelet A, Bourdrez X, Andries K.** 2011. Diarylquinolines, synthesis pathway and quantitative structure-activity relationship studies leading to the discovery of TMC207. Future Med. Chem. **3**:1345–1360.
2. **Iino R, Hasegawa R, Tabata KV, Noji H.** 2009. Mechanism of inhibition by C-terminal α-helices of the ε subunit of *Escherichia coli* F_OF_1-ATP synthase. J. Biol. Chem. **284**:17457–17464.
3. **Barry CE, Boshoff HI, Dartois V, Dick T, Ehrt S, Flynn J, Schnappinger D, Wilkinson RJ, Young D.** 2009. The spectrum of latent tuberculosis: rethinking the biology and intervention strategies. Nat. Rev. Microbiol. 7:845–855.
4. **Diacon AH, Pym A, Grobusch M, Patientia R, Rustomjee R, Page-Shipp L, Pistorius C, Krause R, Bogoshi M, Churchyard G, Venter A, Allen J, Palomino JC, De Marez T, van Heeswijk RPG, Lounis N, Meyvisch P, Verbeeck J, Parys W, de Beule K, Andries K, Neeley DFM.** 2009. The diarylquinoline TMC207 for multidrug-resistant tuberculosis. N. Engl. J. Med. **360**:2397–2405.
5. **Koul A, Dendouga N, Vergauwen K, Molenberghs B, Vranckx L, Willebrords R, Ristic Z, Lill H, Dorange I, Guillemont J, Bald D, Andries K.** 2007. Diarylquinolines target subunit c of mycobacterial ATP synthase. Nat. Chem. Biol. **3**:323–324.

6. **Koul A, Vrankx L, Dendouga N, Balemans W, Van den Wyngaert I, Vergauwen K, Göhlmann HW, Willebrords R, Poncelet A, Guillemont J, Bald D, Andries K.** 2008. Diarylquinolines are bactericidal for dormant mycobacteria as a result of disturbed ATP homeostasis. J. Biol. Chem. **283**:25273–25280.
7. **Rao SP, Alonso S, Rand L, Dick T, Pethe K.** 2008. The protonmotive force is required for maintaining ATP homoeostasis and viability of hypoxic, nonreplicating *Mycobacterium tuberculosis*. Proc. Natl. Acad. Sci. U. S. A. **105**:11945–11950.
8. **Andries K, Verhasselt P, Guillemont J, Göhlmann HWH, Neefs JM, Winkler H, Van Gestel J, Timmerman P, Zhu M, Lee E, Williams P, de Chaffoy D, Huitric E, Hoffner S, Cambau E, Truffot-Pernot C, Lounis N, Jarlier V.** 2005. A diarylquinoline drug active on the ATP synthase of *Mycobacterium tuberculosis*. Science **307**:223–227.
9. **Tran SL, Cook GM.** 2005. The F_1F_O-ATP synthase of *Mycobacterium smegmatis* is essential for growth. J. Bacteriol. **187**:5023–5028.
10. **Bald D, Koul A.** 2010. Respiratory ATP synthases: the new generation of mycobacterial drug target? FEMS Microbiol. **308**:1–7.
11. **Müller V, Lingl A, Lewalter K, Fritz M.** 2005. ATP synthases with novel rotor subunits: new insights into structure, function and evolution of ATPases. J. Bioenerg. Biomembr. **37**:455–460.
12. **Capaldi RA, Aggeler R, Wilkens S, Grüber G.** 1996. Structural changes in the gamma and epsilon subunits of the *Escherichia coli* F_1F_O-type ATPase during energy coupling. J. Bioenerg. Biomembr. **28**:397–401.
13. **Hausrath A, Grüber G, Matthews BW, Capaldi RA.** 1999. Structural features of the γ subunit of the *Escherichia coli* F_1 ATPase revealed by a 4.4-Å resolution map obtained by x-ray crystallography. Proc. Natl. Acad. Sci. U. S. A. **96**:13697–13702.
14. **Uhlin U, Cox GB, Guss JM.** 1997. Crystal structure of the epsilon subunit of the proton-translocating ATP synthase from *Escherichia coli*. Structure **5**:1219–1230.
15. **Wilkens S, Capaldi RA.** 1998. Solution structure of the ε subunit of the F_1-ATPase from *Escherichia coli* and interactions of this subunit with β subunits in the complex. J. Biol. Chem. **273**:26645–26651.
16. **Yagi H, Kajiwara N, Tanaka H, Tsukihara T, Kato-Yamada Y, Yoshida M, Akutsu H.** 2007. Structures of the thermophilic F_1-ATPase ε subunit suggesting ATP-regulated arm motion of its C-terminal domain in F_1. Proc. Natl. Acad. Sci. U. S. A. **104**:11233–11238.
17. **Cingolani G, Duncan TM.** 2011. Structure of the ATP synthase catalytic complex (F(1)) from *Escherichia coli* in an autoinhibited conformation. Nat. Struct. Mol. Biol. **18**:701–708.
18. **Gledhill JR, Montgomery MG, Leslie AG, Walker JE.** 2007. How the regulatory protein, IF1, inhibits F_1-ATPase from bovine mitochondria. Proc. Natl. Acad. Sci. U. S. A. **104**:15671–15676.
19. **Kato-Yamada Y, Yoshida M.** 2003. Isolated epsilon subunit of thermophilic F_1-ATPase binds ATP. J. Biol. Chem. **278**:36013–36016.
20. **Richter ML.** 2004. Gamma-epsilon interactions regulate the chloroplast ATP synthase. Photosynth. Res. **79**:319–329.
21. **Saita E, Iino R, Suzuki T, Feniouk BA, Kinosita K, Yoshida M.** 2010. Activation and stiffness of the inhibited states of F1-ATPase probed by single-molecule manipulation. J. Biol. Chem. **285**:11411–11417.
22. **Grüber G, Godovac-Zimmermann J, Link TA, Coskun Ü, Rizzo VF, Betz C, Bailer SM.** 2002. Expression, purification, and characterization of subunit E, an essential subunit of the vacuolar ATPase. Biochem. Biophys. Res. Commun. **298**:383–391.
23. **Priya R, Biuković G, Gayen S, Vivekanandan S, Grüber G.** 2009. NMR solution structure of the b_{30-82} domain of subunit *b* of *Escherichia coli* F_1F_O ATP synthase. J. Bacteriol. **191**:7538–7544.
24. **Basak S, Gayen S, Thaker YR, Manimekalai MSS, Roessle M, Hunke C, Grüber G.** 2011. Solution structure of subunit F (Vma7p) of the eukaryotic V_1V_O ATPase from *Saccharomyces cerevesiae* derived from SAXS and NMR spectroscopy. Biochim. Biophys. Acta **1808**:360–368.
25. **Roessle M, Klaering R, Ristau U, Robrahn B, Jahn D, Gehrmann T, Konarev PV, Round A, Fiedler S, Hermes S, Svergun DI.** 2007. Upgrade of the small angle X-ray scattering beamline X33 at the EMBL Hamburg. J. Appl. Crystallogr. **40**:190–194.
26. **Svergun D.** 1993. A direct indirect method of small-angle scattering data treatment. J. Appl. Cryst. **26**:258–267.
27. **Guinier A, Fournet G.** 1955. Small-angle scattering of X-ray, Wiley, New York, NY.
28. **Svergun DI, Bećirević A, Schrempf H, Koch MHJ, Grüber G.** 2000. Solution structure and conformational changes of the streptomyces chitin binding protein (CHB1). Biochemistry **39**:10677–10683.
29. **Volkov VV, Svergun DI.** 2003. Uniqueness of ab initio shape determination in small angle scattering. J. Appl. Cryst. **36**:860–864.
30. **Güntert P.** 2004. Automated NMR structure calculation with CYANA. Methods Mol. Biol. **278**:353–378.
31. **Kumar A, Manimekalai MSS, Balakrishna AM, Jeyakanthan J, Grüber G.** 2010. Nucleotide binding states of subunit A of the A-ATP synthase and the implication of P-loop switch in evolution. J. Mol. Biol. **396**:301–320.
32. **Suzuki T, Wakabayashi C, Tanaka K, Feniouk BA, Yoshida M.** 2011. Modulation of nucleotide specificity of thermophilic F_OF_1-ATP synthase by ε subunit. J. Biol. Chem. **286**:16807–16813.
33. **Berjanskii MV, Neal S, Wishart DS.** 2006. PREDITOR: a web server for predicting protein torsion angle restraints. Nucleic Acids Res. **34**:63–69.
34. **Haagsma AC, Podasca I, Koul A, Andries K, Guillemont J, Lill H, Bald D.** 2011. Probing the interaction of the diarylquionline TMC207 with its target mycobacterial ATP synthase. PLoS One **6**:e23575. doi:10.1371/journal.pone.0023575.
35. **Wishart DS, Sykes BD, Richards FM.** 1991. Relationship between nuclear magnetic resonance chemical shift and protein secondary structure. J. Mol. Biol. **222**:311–333.
36. **Martín-Galiano AJ, Gorgojo B, Kunin CM, de la Campa AG.** 2002. Mefloquine and new related compounds target the F_0 complex of the F_0F_1 H^+-ATPase of *Streptococcus pneumoniae*. Antimicrob. Agents Chemother. **46**:1680–1687.
37. **Haagsma AC, Driessen NN, Hahn MM, Lill H, Bald D.** 2010. ATP synthase in slow- and fast-growing mycobacteria is active in ATP synthesis and blocked in ATP hydrolysis direction. FEMS Microbiol. Lett. **313**:68–74.
38. **Via LE, Lin PL, Carrillo J, Allen SS, Eum SY, Taylor K, Klein E, Manjunatha U, Ganzales J, Lee EG, Park SK, Raleigh JA, Cho SN, McMurray DN, Flynn JL, Barry CE III.** 2008. Tuberculous granulomas are hypoxic in guinea pigs, rabbits, and nonhuman primates. Infect. Immun. **76**:2333–2340.
39. **Zharova TV, Vinogradov AD.** 2004. Energy-dependent transformation of $F_0.F_1$-ATPase in *Paracoccus denitrificans* plasma membranes. J. Biol. Chem. **279**:12319–12324.
40. **Grüber G, Godovac-Zimmermann J, Nawroth T.** 1994. ATP synthesis and hydrolysis of the ATP-synthase from *Micrococcus luteus* regulated by an inhibitor subunit and membrane energization. Biochim. Biophys. Acta **1186**:43–51.
41. **Mendel-Hartvig J, Capaldi RA.** 1991. Nucleotide-dependent and dicyclohexyl-carbodiimide-sensitive conformational changes in the ε subunit of *Escherichia coli* ATP synthase. Biochemistry **30**:10987–10991.
42. **Grüber G, Engelbrecht S, Junge W, Dose K, Nawroth T.** 1994. Purification and characterization of the inhibitory subunit δ of the ATP-synthase from *Micrococcus luteus*. FEBS Lett. **356**:226–228.
43. **Kaneko T, Cooper C, Mdluli K.** 2011. Challenges and opportunities in developing novel drugs for TB. Future Med. Chem. **3**:1373–1400.
44. **Morales-Ríos E, de la Rosa-Morales F, Mendoza-Hernández G, Rodríguez-Zavala JS, Celis H, Zarco-Zavala M, García-Trejo JJ.** 2010. A novel 11-kDa inhibitory subunit in the F_1F_O ATP synthase of *Paracoccus denitrificans* and related alpha-proteobacteria. FASEB J. **24**:599–608.
45. **Dmitriev O, Jones PC, Jjiang W, Fillingame RH.** 1999. Structure of the membrane domain of subunit b of the Escherichia coli FOF1 ATP synthase. J. Biol. Chem. **274**:15598–15604.
46. **Priya R, Tadwal SV, Roessle M, Gayen S, Hunke C, Peng WC, Torres J, Grüber G.** 2008. Low resolution structure of subunit b (b_{22-156}) of *Escherichia coli* F_1F_o ATP synthase in solution and the b–δ assembly. J. Bioenerg. Biomembr. **40**:245–255.